Analysis of the constituents of urinary calculi of dog using various scientific techniques

Pragnya A. Bhatt[1], Riddhi P. Laiya[1], Deepak B. Patil[2], Pinesh V. Parikh[2] and Parimal Paul[1,*]

[1]Analytical Discipline and Centralized Instrument Facility, CSIR-Central Salt and Marine Chemicals Research Institute, G.B. Marg, Bhavnagar 364 002, India
[2]College of Veterinary Science and Animal Husbandry, Anand Agricultural University, Anand 388 001, India

Analytical techniques have been used to determine constituents of urinary stones of different breeds of dogs obtained from the College of Veterinary Science and Animal Husbandry, Anand Agricultural University, India. Analysis by powder XRD, FTIR and TGA suggests the presence of pure phases such as calcium oxalate monohydrate, struvite and calcium carbonate, and also mixed phases containing calcium oxalate hydrate, struvite, whewellite and weddellite in the urinary calculi. The morphology of the constituents has been studied by optical and scanning electron microscope. Activation energy and order of reaction for thermal elimination of H_2O, CO and CO_2 have been determined.

Keywords: Analytical techniques, dogs, powder X-ray diffraction, urinary calculi.

UROLITHIASIS and other diseases related to urinary stone are common in human beings and in small animals like dogs and cats throughout the world. Various techniques are being used for the removal of stones found in dogs and cats[1–4]. Urolithiasis in dogs has also been studied by several research groups addressing various causes of stone formation, analysis of the constituents of stones and also therapeutic aspects of the disease[5–9]. For all of these studies and follow up treatment, it is necessary to know the constituents of the urinary calculi and significant progress has been made in this direction by studying the removed calculi using various analytical techniques[10–18]. In this regard, the Veterinary Urolith Center in Canada has done considerable work and has reported analysis of urinary calculi of dogs; however, details of analytical techniques used have not been mentioned[14]. Analysis of calculi of dogs has also been reported by other groups and in some cases ultra-structure of the urinary calculi has also been reported[15–17].

The characterization of the constituents of urinary calculi is not only important for the treatment of stone-related diseases, but it also helps to understand the mechanism of stone formation and how it is related to food habits and other environmental effects of dogs of different breeds and regions. To the best of our knowledge no such systematic analytical study has been carried out in India, though a large number of breeds of dogs are found in the country. This kind of study has now become more informative with the advancement of analytical instruments, which give detailed and accurate analysis of the constituents of analyte phase, morphology, structural aspects and temperature-dependent phase transition[18].

In the present study, analysis of the mineral contents of nine urinary calculi of dogs has been reported. The analysis was carried out using powder X-ray diffractometer (XRD), Fourier transform infrared spectrometer (FT-IR), thermogravimetric analysis (TGA) and scanning electronmicroscope (SEM). Dehydration data obtained from TGA were also used to determine solid-state reaction kinetics of calcium oxalate monohydrate and struvite, which is a new type of study in the case of urinary calculi.

The urinary stones were obtained from a surgeon (D.B.P.) from the College of Veterinary Science and Animal Husbandry, Anand Agricultural University, Gujarat, India. The urinary calculi were surgically removed from the dogs following the standard procedure reported by Fossum *et al.*[19].

Optical images were recorded on an optical microscope (Olympus, model BX 16) Powder XRD measurements were performed on a Philips X'PERT MPD X-ray powder diffractometer, using CuKα radiation in the 2θ range 10–80°. Phase identification of each of the samples was carried out using the Search-Match analysis of Highscore Plus software. The analysis was performed using ICDD database. FTIR analysis was performed on a Perkin Elmer Spectrum GX FTIR system using KBr pellet. SEM images were recorded on Carl Zeiss SMT Leo 1430 VP with operating voltage of 5 and 15 kV. TGA was carried out on a Metler Toledo TGA system; the measurement was performed with the heating rate of 2, 5 and 10°/min under nitrogen atmosphere.

Optical images of the samples were recorded (40×) using a microscope. Figure 1 shows the images of two samples, UC-Dog-2 and UC-Dog-3. It may be noted that the morphology of the samples is markedly different; the
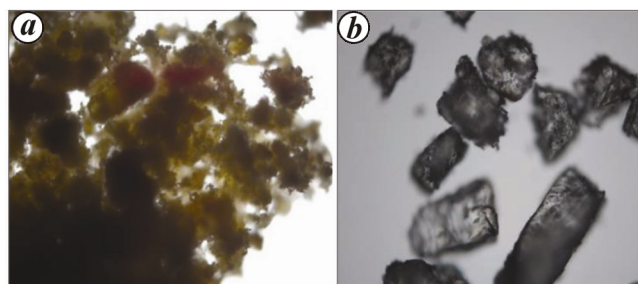
Figure 1. Optical microscopic images of the samples: *a*, UC-Dog-2; *b*, UC-Dog-3.

*For correspondence. (e-mail: ppaul@csmcri.org)

Table 1. Phase identification based on PXRD Search-Match analysis

Sample code	Breed	Age (years)	Matched phases	Chemical formula	ICDD-JCPDF number
UC-Dog-1	Dalmatian	–	Calcium oxalate monohydrate (COM)	$CaC_2O_4 \cdot H_2O$	00-020-0231
UC-Dog-2	Dobermann	–	COM	$CaC_2O_4 \cdot H_2O$	00-020-0231
UC-Dog-3	Dobermann Pinscher	8	Struvite	$NH_4MgPO_4 \cdot 6H_2O$	00-015-0762
UC-Dog-4	Dachshund	7	Struvite	$NH_4MgPO_4 \cdot 6H_2O$	98-001-4269
UC-Dog-5	Dalmatian	6	Calcium carbonate	$CaCO_3$	01-085-0849
UC-Dog-6	Pug	1.5	Struvite	$NH_4MgPO_4 \cdot 6H_2O$	98-006-0626
			COM		00-020-0233
			Calcium oxalate hydrate	$CaC_2O_4 \cdot H_2O$	04-008-9822
				$CaC_2O_4\ 2.25H_2O$	
UC-Dog-7	Spitz	7	Struvite	$NH_4MgPO_4 \cdot 6H_2O$	98-001-4269
UC-Dog-8	Dobermann	12	Whewellite	$CaC_2O_4 \cdot H_2O$	00-020-0231
	Pinscher		Weddellite	$CaC_2O_4\ 2H_2O$	04-011-6807
UC-Dog-9	Pomeranian	10	Struvite	$NH_4MgPO_4 \cdot 6H_2O$	98-001-4269
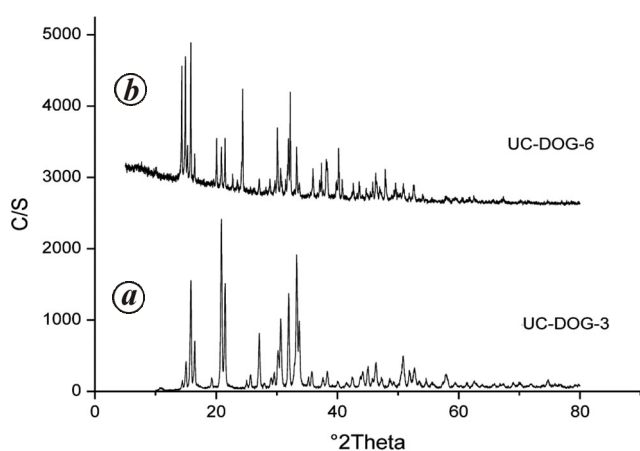
Figure 2. Powder X-ray diffractograms of the samples: *a*, UC-Dog-3; *b*, UC-Dog-6.
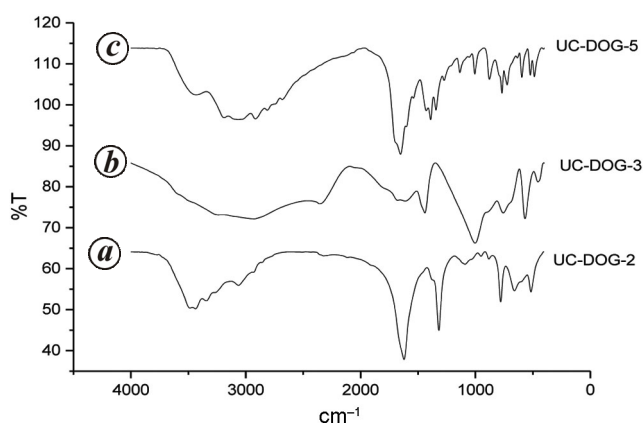
Figure 3. Infrared spectra of the samples: *a*, UC-Dog-2; *b*, UC-Dog-3; *c*, UC-Dog-5.

image of UC-Dog-2 (Figure 1 *a*) shows aggregated grains of undefined shape and sizes, whereas that of UC-Dog-3 (Figure 1 *b*) shows crystals with distinct grains of definite shape and size such as square, rectangular, etc.

For characterization of the constituents of the urinary calculi, powder XRD pattern of the samples was recorded. Figure 2 shows the diffractograms of the samples UC-Dog-3 and UC-Dog-6 respectively. Search-Match analysis of data of all samples was performed using Highscore Plus software and the results are given in Table 1. The table lists the sample code, sample description, chemical name of the matched phases, chemical formula and the respective reference numbers (ICDD-JCPDF). The analysis revealed the presence of pure phases, viz. calcium oxalate monohydrate, struvite and calcium carbonate (UC-Dog-1, UC-Dog-2, UC-Dog-3, UC-Dog-4, UC-Dog-5 and UC-Dog-7 and UC-Dog-9), as well as mixed phases containing different combinations of calcium oxalate hydrate, struvite, whewellite and weddellite (UC-Dog-6 and UC-Dog-8).

Infrared spectra of all the samples were recorded. Figure 3 *a–c* shows the spectra of the samples UC-Dog-2, UC-Dog-3 and UC-Dog-5 respectively. It may be noted that though all the three samples are urinary calculi, the IR spectra are distinctly different, which is consistent with the powder XRD observation. The spectrum of UC-Dog-2 (Figure 3 *a*) matches well with the reported spectrum for calcium oxalate monohydrate[18], and it is consistent with the observation noted by phase identification of the powder XRD data (ICDD-JCPDF number 00-020-0231; Table 1). The broad band centring around 3500 cm^{-1} is due to the water molecule, while the two sharp and strong bands at 1625 and 1320 cm^{-1} are due to ν(C=O) and ν(C–O) respectively[18]. The band at 878 cm^{-1} may be assigned to the C–C stretching mode. The IR spectrum of UC-Dog-3 (Figure 3 *b*) matches with that reported for ammonium magnesium phosphate hexahydrate (struvite)[20]. The broad band in the range 3500–3000 cm^{-1} is due to the H_2O and NH_4^+ groups. The band at 2927 cm^{-1} is due to antisymmetric stretching vibrations of NH_4^+ group. While those at 1003, 568 and 455 cm^{-1} are assigned to the PO_4^{3-} group[20]. Bands in the range 1600–1400 cm^{-1} are those of H–N–H deformation mode of NH_4^+ (ref. 20). The spectrum of UC-Dog-5 exhibited characteristic bands of

calcite[21] at 724, 878 and 1428 cm^{-1}; these bands are assigned to ν_4 plane bending, ν_2 out of plane bending and ν_3 asymmetric stretching respectively.

Optical images for UC-Dog-2 and UC-Dog-3 are distinctly different (Figure 1). To study the morphology, SEM images of these samples were recorded. The SEM images of UC-Dog-1 and UC-Dog-3 (Figure 4 a and b respectively) clearly exhibited distinctly different morphology, which is consistent with the finding of different constituents (calcium oxalate monohydrate and struvite) in the samples UC-Dog-1 and UC-Dog-3; similar observation of existence of mixed phases has also been reported by others[22].

TGA of the constituents with pure phases was also carried out to study the changes in terms of mass loss with increasing temperature. Figure 5 a and b shows the thermograms of the samples, UC-Dog-2 (calcium oxalate monohydrate) and UC-Dog-3 (struvite) respectively. It may be noted that UC-Dog-2 exhibit mass loss in three stages (Figure 5 a), whereas UC-Dog-3 showed it in a single stage (Figurer 5 b). Table 2 provides details of the mass loss in different stages. We also determined the activation energy for the loss of H_2O, CO and CO_2 from TGA data using the Coats and Redfern equation[23] shown

below, following the procedure mentioned in the literature[22,24].

$$\log_{10}\left(\frac{1-(1-\alpha)^{1-n}}{T^2(1-n)}\right) = \left\{\log_{10}\left(\frac{AR}{\alpha E}\right)\left(1-\frac{2RT}{E}\right) - \left(\frac{E}{2.3RT}\right)\right\},$$
$$\text{(for } n \neq 1), \tag{1}$$

$$-\log_{10}\left[-\frac{\log(1-\alpha)}{T^2}\right] = \log_{10}\left[\frac{AR}{\alpha E}\right]\left[1-\frac{2RT}{E}\right] - \left\{\frac{E}{2.3RT}\right\},$$
$$\text{(for } n = 1). \tag{2}$$

where E is the activation energy of the reaction, A the frequency factor, α the fraction of decomposed material at time t, n the order of reaction and T is the absolute temperature. The slope of the plot of $Y = -\log_{10}[\{1 - (1-\alpha)^{1-n}\}/\{T^2(1-\alpha)\}]$ versus $X = 1/T$ of eq. (1) equals to $m = E/2.3RT$. R is the gas constant and T is known, therefore activation energy (E) can be calculated from the TGA data. For the sample UC-Dog-2, eq. (1) is applied for each rate and for all the three stages, viz. loss of H_2O, CO and CO_2. Figure 6 shows the plots and the linear fits. From the slope of the best-fit plots, the activation energy can be calculated (Table 3). Table 4 gives the activation energy determined for H_2O elimination for three different rates.

The optical microscopic images suggest that the physical appearance of the samples may differ significantly depending on the constituents present in them. Similarly, SEM images indicate constituents-based differences in morphology. The powder XRD results indicate a wide range of variation in the mineral contents of urinary calculi, which are common constituents usually reported in urinary calculi of dogs[25]. The IR data are consistent with the findings made by the powder XRD analysis. The three-stage mass losses for UC-Dog-2 are due to loss of H_2O, CO and CO_2, which is consistent with the reported

Figure 4. Scanning electron microscope images of the samples: **a**, UC-Dog-1; **b**, UC-Dog-3.
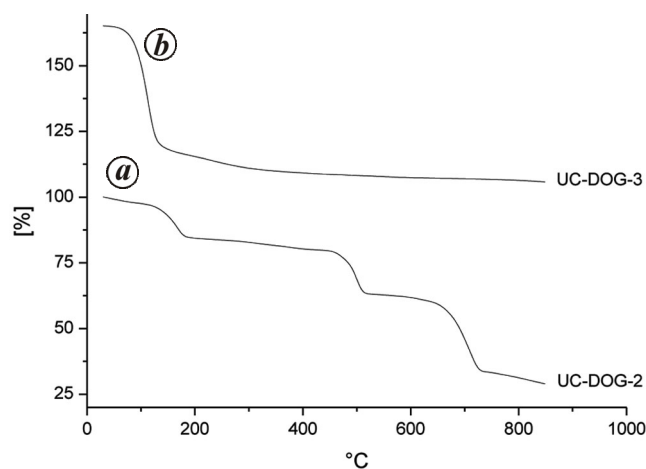
Figure 5. Thermogravimetric analysis of the samples: **a**, UC-Dog-2; **b**, UC-Dog-3.

Table 2. Experimental and calculated mass loss (%) by thermogravimetric analysis

Sample-ID	Weight loss (%)					
	Stage-1		Stage-2		Stage-3	
UC-Dog-2-1	10.95	12.30[a]	15.28	19.10[b]	26.11	30.10[c]
UC-Dog-3	50.24	51.00[d]				

[a]Calculated % for H_2O; [b]Calculated % for CO; [c]Calculated % for CO_2; [d]Calculated % for H_2O and NH_3.

Table 3. Order of reaction (n) and activation energy (E) for calcium oxalate monohydrate decomposition

Sample-code	n	M (slope)	E (kcal/mol)
UC-Dog-2-H_2O	0.71	2.14	9.78
UC-Dog-2-CO	0.38	2.69	12.30
UC-Dog-2-CO_2	0.46	2.16	9.87

Table 4. Activation energy for H_2O removal from UC-Dog-2 stone at various heating rates

Heating rate (°C/m)	Sample-code	n	Linear equation	R^2	E (kcal/mol)
2	UC-Dog-H_2O-	0.66	$Y = 1.903X + 1.684$	0.99	8.69
5	UC-Dog-H_2O	0.66	$Y = 2.059X + 1.356$	0.99	9.41
10	UC-Dog-H_2O-	0.66	$Y = 1.590X + 2.850$	0.93	7.26
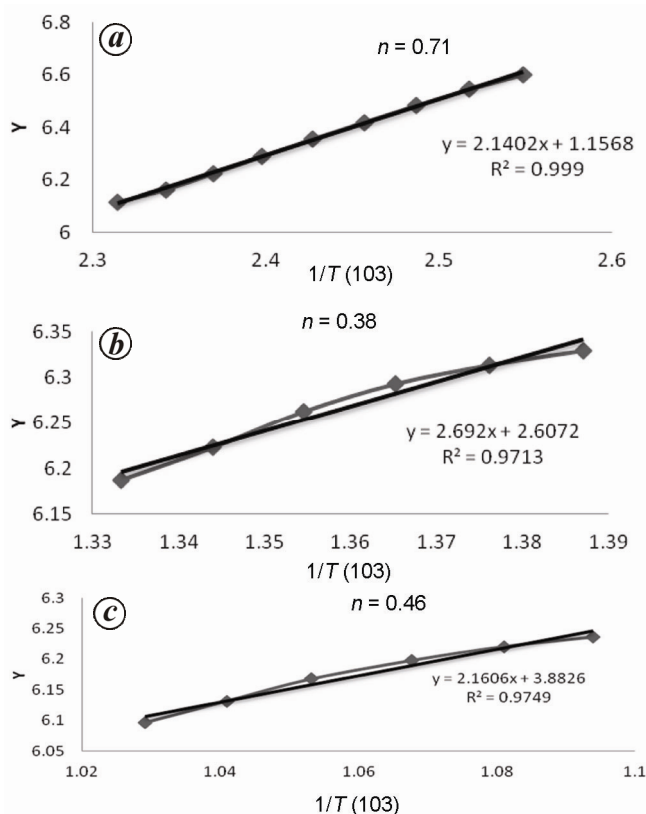
Figure 6. Coats and Redfern plots of sample UC-Dog-2: *a*, for H_2O; *b*, for CO; *c*, for CO_2.

data for calcium oxalate monohydrate containing stones[18]. As shown in Table 2, the experimental values of mass loss match well with the calculated values for H_2O. However, for CO and CO_2 considerable deviation is noted, which is probably due to the presence of some minor organic constituents in the samples. Figure 5 *b* shows a broad single-stage mass loss of 50.24% in the temperature range 40–200°C for UC-Dog-3. This is in agreement with reported data for struvite[26]. This mass loss is due to the simultaneous release of $6H_2O$ and NH_3; the calculated value for this (51%) is close to the observed data. Table 3 shows the activation energy for removal of each of the three molecules, namely H_2O, CO and CO_2. It may be noted that the activation energy obtained for these three molecules is considerably low compared to that reported for some other systems[24]. This may be attributed to the probability of comparatively favourable environment for mineral decomposition to take place in the presence of interwoven organic matrix. It may be noted from Table 4

that the rate of measurement of TGA data does not have significant effect on order of reaction (*n*) and activation energy (*E*) for elimination of H_2O.

The mineral constituents of nine urinary calculi of different breeds of dogs have been characterized on the basis of powder XRD, FTIR, TGA, SEM and optical microscopic studies. Analysis of powder X-ray data revealed the presence of pure as well as mixed phase constituents in the stones. The pure phases are calcium oxalate monohydrate, struvite and calcium carbonate, and the mixed phases contain different combinations of calcium oxalate hydrate, struvite, whewellite and weddellite. The powder XRD findings were supported by IR and TGA analysis. SEM images clearly demonstrated different morphology depending on the constituents present in the stones. The TGA data were used to calculate the activation energy for thermal elimination of H_2O, CO and CO_2 from the stones. The present study demonstrates the instrument-based analytical methods which can be employed for the analysis of urinary calculi of dogs. The findings also suggest that the constituents of the urinary calculi differ significantly in different breeds. Thus, such type of study may help rationalize the observation in terms of food habit, environment, age and breed of the dog.

Conflict of interest statement. None of the authors of this paper has a financial or personal relationship with other people or organizations that could inappropriately influence or bias the contents of this manuscript.

1. Defarges, A. and Dunn, M., Use of electrohydraulic lithotripsy in 28 dogs with bladder and urethral Calculi. *J. Vet. Intern. Med.*, 2008, **22**, 1267–1273.
2. Osborne, C. A. *et al.*, Feline lower urinary tract diseases. In *Textbook of Veterinary Internal Medicine* (ed. Ettinger, E. C.), 2005.
3. Lulich, J. P., and Osborne, C. A., Catheter assisted retrieval of urocystoliths from dogs and cats. *J. Am. Vet. Med. Assoc.*, 1992, **201**, 111–113.
4. Lulich, J. P. *et al.*, Nonsurgical removal of urocystoliths in dogs and cats by voiding urohydropropulsion. *J. Am. Vet. Med. Assoc.*, 1993, **203**, 660–663.
5. Moryama, M. T., Manabu, T., Chizue Domiki, Katsuhito Miyazawa K., Tanaka, T. and Suzuki, K., Effects of oxalate exposure on Madin–Darby canine kidney cells in culture, renal prothrombin fragment-1 mRNA expression. *Urol. Res.*, 2005, **33**, 470–475.
6. Piperisova, I., Jennifer A. N. and Papich, M. G., What is your diagnosis? Marked hyperchloremia in a dog. *Vet. Clin. Pathol.*, 2009, **38**, 411–414.
7. Wynn, V. M., Davidson, E. B., Higbee, R. G., Ritchey, J. W., Ridgway, T. D., Bartels, K. E. and Lucroy, M. D., *In vitro* effects of pulsed holmium laser energy on canine uroliths and porcine cadaveric urethra. *Lasers Surg. Med.*, 2003, **33**, 243–246.

8. Gatoria, I. S., Saini, N. S., Rai, T. S. and Dwivedi, P. N., Comparison of three techniques for the diagnosis of urinary tract infections in dogs with urolithiasis. *J. Small Anim. Pract.*, 2006, **47**, 727–732.

9. Agut, A., Lucas, X., Castro, A., De Membiela, F., Soler, M. and Belda, E., A urethrorectal fistula due to prostatic abscess associated with urolithiasis in a dog. *Reprod. Dom. Anim.*, 2006, **41**, 247–250.

10. Bovee, K. C. and McGuire, T., Qualitative and quantitative analysis of uroliths in dogs. Definitive determination of chemical type. *J. Am. Vet. Med. Assoc.*, 1984, **185**, 983–987.

11. Osborne, C. A., Clinton, C. W., Moran, H. C. and Bailie, N. C., Comparison of qualitative and quantitative analysis of canine uroliths. *Vet. Clin. North Am. Small Anim. Pract.*, 1986, **16**, 317–323.

12. Ruby, A. L. and Ling, G. V., Methods of analysis of canine uroliths. *Vet. Clin. North Am. Small Anim. Pract.*, 1986, **16**, 293–301.

13. Houston, D. M., Moore, A. E., Favrin, M. G. and Brent, H., Feline urethral plugs and bladder uroliths, a review of 5484 submissions, 1998–2003. *Can. Vet. J.*, 2003, **44**, 974–977.

14. Houston, D. M., Moore, A. E., Favrin, M. G. and Brent, H., Canine urolithiasis: a look at over 16,000 urolith submissions to the Canadian Veterinary Urolith Centre from February 1998 to April 2003. *Can. Vet. J.*, 2004, **45**, 225–230.

15. Escolar, E., Bellanato, J. and Rodriquez, M., Study of cystien urinary calculi in dogs. *Can. J. Vet. Res.*, 1991, **55**, 67–70.

16. Domingo-Neumann, R. A., Ruby, A. L., Ling, G. V., Schiffman, P. S. and Johnson, D. L., Ultrastructure of selected struvite-containing urinary calculi from dogs. *Am. J. Vet. Res.*, 1996, **57**(9), 1274–1287.

17. Rodgers, A. L., Mezzabotta, M., Mulder, K. J. and Nassimbeni, L. R., Application of several physical techniques in the total analysis of a canine. Urinary calculus. *J. S. Afr. Vet. Assoc.*, 1981, **2**, 139–142.

18. Bhatt, P. A. and Paul, P., Analysis of urinary stone constituents using powder X-ray diffraction and FT-IR. *J. Chem. Sci.*, 2008, **120**, 267–273.

19. Fossum, T. W. *et al.*, *Small Animal Surgery,* Mosby Elsevier. Missouri, 2002, 3rd edn, pp. 663–701.

20. Kurtulus, G. and Tas, A. C., Transformations of neat and heated struvite. *Mater. Lett.*, 2011, **65**, 2883–2886.

21. Plavsic, B., Kobe, S. and Orel, B., Identification of crystallization forms of $CaCO_3$ with FTIR spectroscopy. *KZLTET*, 1999, **33**(6), 517–521.

22. Chauhan, C. K., Joseph, K. C., Parekh, B. B. and Joshi, M. J., Growth and characterization of struvite. *Indian J. Pure Appl. Phys.*, 2008, **46**, 507–512.

23. Coats, A. W. and Redfern, J. P., Kinetic parameters from thermogravimetric Data. *Nature*, 1964, **201**, 68.

24. Joshi, V. S. and Joshi, M. J., FTIR spectroscopic, thermal and growth morphological studies of calcium hydrogen phosphate dihydrate crystals. *Cryst. Res. Technol.*, 2003, **38**, 9.

25. Osborne, C. A. *et al.*, Analysis of 77,000 canine uroliths, perspective from the Minnesota Urolith Center. *Vet. Clin. North Am. Small Anim. Pract.*, 1999, **29**(1), 17–38.

26. Teresa, P., Lozano-Garcia, S., Caballero-Miranda, M., Ortega-Guerrero, B. and Roy, P., Discovery and characterization of a struvite layer in the paleolake, Mexico. *Rev. Mex. Cienc. Geol.*, 2010, **27**(3), 573–580.

Economic analysis of different greenhouse gas mitigation technologies in rice–wheat cropping system of the Indo-Gangetic Plains

Dipak Kumar Gupta[1],*, Arti Bhatia[1], T. K. Das[2], Parmendra Singh[2], Amit Kumar[1], Niveta Jain[1] and Himanshu Pathak[1]

[1]Centre for Environment Science and Climate Resilient Agriculture, and [2]Division of Agronomy, ICAR-Indian Agricultural Research Institute, New Delhi 110 012, India

To reduce the greenhouse gas (GHG) emission from rice and wheat cultivation several mitigation options have been suggested. However, economic impact of these technologies has been poorly documented. In the present study economic analysis of some emerging GHG mitigation technologies for rice–wheat system of the Indo-Gangetic Plains has been carried out. The experiment consisted of six combinations of wheat–rice crop rotation using eight treatments, including conventionally tilled wheat (CTW), zero tilled wheat (ZTW), transplanted puddled rice (TPR), dry direct seeded rice (DSR), intermittent wetting and drying (IWD), application of rice straw (RS) with ZTW and use of neem oil-coated urea (NOCU) in TPR and ZTW. Cost of various inputs and income from grain and straw were used for computing the benefit to cost (B : C) ratio in the different treatments. ZTW showed higher yield and B : C ratio compared to CTW along with reduction in fuel consumption during tillage operation. In spite of lower yield under DSR and IWD, saving of water, labour and energy in these treatments lowered the cost of cultivation and enhanced B : C ratio similar to TPR. Application of rice straw and NOCU also showed positive impact on crop yield. B : C ratio of rice–wheat system ranged from 1.62 to 1.86 in the first year and from 1.86 to 2.16 in the second year. B : C ratio was significantly higher in all the treatments in the experimented rice–wheat system compared to conventional system, i.e. CTW–TPR. The ZTW + RR – DSR (WR5) showed highest B : C ratio followed by ZTW + DSR (WR4) in both the seasons.

Keywords: Economic analysis, greenhouse gases, mitigation technology, rice–wheat system.

THE rice–wheat cropping system (RWCS) of the Indo-Gangetic Plains (IGP) is crucial for food security in Southeast Asia. This system covers 13.5 m ha of land with high concentration in Indian IGP (10.5 m ha). The Indian IGP occupies about 53% of the total area under RWCS, produces about 50% of the total food grains and feeds almost 40% of the population of our country[1,2].